Mechanics of the Toxoplasma gondii oocyst wall

Aurélien Dumètre, Jitender P. Dubey, David J.P. Ferguson, Pierre Bongrand, Nadine Azas, Pierre-Henri Puech

Mechanics of the Toxoplasma gondii oocyst wall

Aurélien Dumètre[a,1], Jitender P. Dubey[b,1], David J. P. Ferguson[c], Pierre Bongrand[d,e], Nadine Azas[a], and Pierre-Henri Puech[d,1]

[a]Unité Mixte de Recherche (UMR) Ministère de la Défense 3 Infections Parasitaires, Transmission, Physiopathologie et Thérapeutique, Faculté de Pharmacie, Aix-Marseille Université, 13385 Marseille Cedex 05, France; [b]Animal Parasitic Diseases Laboratory, Agricultural Research Service, Beltsville Agricultural Research Center, US Department of Agriculture, Beltsville, MD 20705-2350; [c]Nuffield Department of Clinical Laboratory Science, University of Oxford, John Radcliffe Hospital, Oxford OX3 9DU, United Kingdom; [d]Institut National de la Santé et de la Recherche Médicale U1067/Centre National de la Recherche Scientifique, UMR 7333, Adhésion Cellulaire et Inflammation, Aix-Marseille Université, 13288 Marseille Cedex 09, France; and [e]Laboratoire d'Immunologie, Hôpital de la Conception, 13385 Marseille, France

The ability of microorganisms to survive under extreme conditions is closely related to the physicochemical properties of their wall. In the ubiquitous protozoan parasite Toxoplasma gondii, the oocyst stage possesses a bilayered wall that protects the dormant but potentially infective parasites from harsh environmental conditions until their ingestion by the host. None of the common disinfectants are effective in killing the parasite because the oocyst wall acts as a primary barrier to physical and chemical attacks. Here, we address the structure and chemistry of the wall of the T. gondii oocyst by combining wall surface treatments, fluorescence imaging, EM, and measurements of its mechanical characteristics by using atomic force microscopy. Elasticity and indentation measurements indicated that the oocyst wall resembles common plastic materials, based on the Young moduli, E, evaluated by atomic force microscopy. Our study demonstrates that the inner layer is as robust as the bilayered wall itself. Besides wall mechanics, our results suggest important differences regarding the nonspecific adhesive properties of each layer. All together, these findings suggest a key biological role for the oocyst wall mechanics in maintaining the integrity of the T. gondii oocysts in the environment or after exposure to disinfectants, and therefore their potential infectivity to humans and animals.

oocyst structure | oocyst integrity | oocyst resistance | Toxoplasma infectivity | transmission

Resistance to physical and chemical degradation is essential for the perpetuation of the lifecycle of environmentally exposed microbial pathogens. In the coccidian parasite Toxoplasma gondii, this function is served by the oocyst, the only stage of the parasite structurally equipped to survive in harsh environments (1). Oocyst-related infections in humans and other warm-blooded animals worldwide have been increasingly reported as more prevalent and severe than previously thought (2–6). Infections lead to possible deleterious ocular and neurological complications and even death (7). In this context, a global effort has emerged to decipher the basic structures (8, 9) and biological processes of the oocyst (10–13) that allow the parasite to survive different environmental conditions and disinfectants (14–18).

The oocyst is the result of sexual multiplication of T. gondii in the intestinal epithelium of cats (19–21). A few days postinfection, unsporulated (uninfective) spheroid oocysts (10 × 12 μm) are excreted in cat feces and become rapidly infective following aerobic sporulation (22). Sporulation results in different subpopulations of maturing oocysts during the first few days (22): unsporulated (NS), "sporoblast-staged" (SB), and fully sporulated (SP) oocysts (11, 22). SP oocysts are ovoid, measure 11 × 13 μm in size and have two sporocysts (6 × 8 μm), each containing four infective banana-shaped sporozoites (2 × 6–8 μm) (SI Appendix, Fig. S1) (23, 24).

T. gondii oocysts are highly resistant to environmental influences; this resistance to various physical and chemical stressors, including disinfectants such as UV, ozone, and chlorine-based products, is attributed to the oocyst wall (4, 25, 26). In contrast, oocysts are rapidly inactivated following exposure to temperatures above 60 °C for a few minutes (27). The oocyst wall is bilayered, with the outer layer being thinner than the inner layer (24). The layers are not tightly bound to each other because the outer layer can be stripped off easily using sodium hypochlorite (refs. 10, 12, and 22 and the present study). The oocyst wall is made of more than 90% proteins with several structural cysteine- and tyrosine-rich proteins having been identified in the outer layer only (13) or in whole oocyst wall fractions (10, 12). How these different proteins are processed and/or packed to form the oocyst wall is still not clear (8). Current models support a strong contribution of protein-tyrosine cross-linking in the formation and hardening of the oocyst wall in Toxoplasma-related coccidia (8, 12, 26, 28) and results in the development of its typical blue autofluorescence (AF) under UV excitation (10, 26, 28, 29) (SI Appendix, Fig. S1B). This complex polymeric organization also suggests an important robustness of the T. gondii oocyst wall in terms of mechanics (8, 26). Thus, measuring mechanical properties of the T. gondii oocyst wall appears to be relevant to addressing the respective roles of structure and chemistry of each layer of the oocyst wall in the overall resistance of the oocyst to various physical and chemical agents (8).

Atomic force microscopy (AFM) is a rather new technique in biology that fits perfectly for this purpose (30). AFM provides valuable information regarding the surface topography and/or allows force measurements in physiological media, with fixed or unfixed samples, from proteins to cells (31–33). AFM uses a finger-like tip at the extremity of a very soft cantilever (30). This tip can be used to: (i) delineate the surface (imaging mode; refs. 34–36), (ii) indent objects' surface by pressing on them and allowing measurement of their mechanical properties (force mode, mechanics) (37–40), or (iii) probe the adhesion of surface molecules when decorated with suitable haptens and pulling the lever off the surface until all built bridges are broken. This allows direct quantifying of the force that these bridges can sustain (force mode, adhesion). For modes ii and iii, the AFM cantilever is held at a given x,y above the sample (a surface or a cell) and ramped in z-direction. Measuring cantilever deflection as a function of piezo position produces force-extension curves (FC) (30).

Using the AFM tip as a microindentor and using the part of the FC where the tip is pressed on the surface, one can gain information regarding the local elastic properties as measured as a Young's modulus, E, using a Hertz model for elastic indentation. E moduli measured for different eukaryotic cell types vary greatly from cell type to cell type and usually range from 1 kPa to several hundred kilopascals (37, 38). Using the part of the FC where the tip is retracted from the surface, adhesion force measurements can be performed and have been used in cell

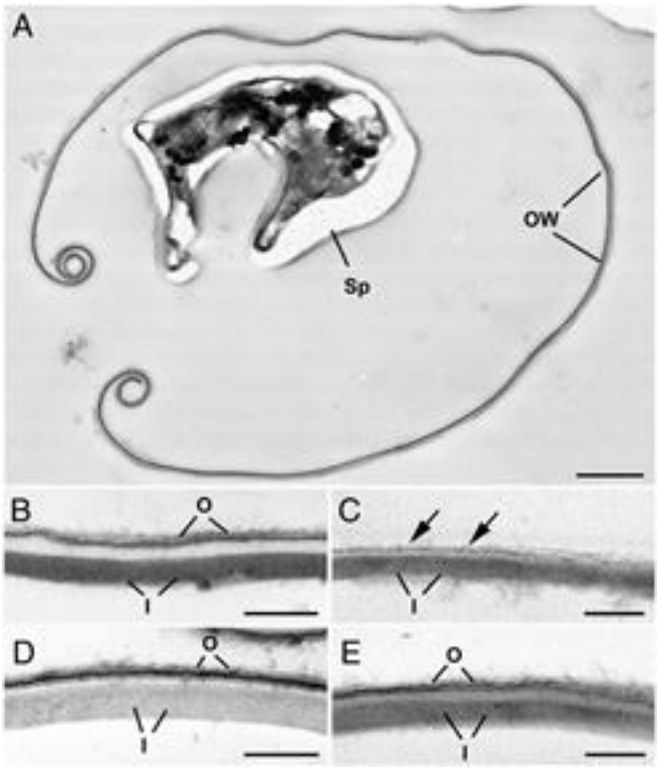

Fig. 1. Ultrastructure of the T. gondii oocyst wall. (A) Low-magnification image of a control (water maintained) oocyst showing the ruptured oocyst wall (OW) and the remnants of a sporocyst (Sp). Bar is 1 μm. (B) Detail of the oocyst wall from a control oocyst showing the thinner outer layer (O) and the thicker inner layer (I). Bar is 100 nm. (C) Detail of the oocyst wall from a bleached oocyst showing the inner layer (I) with loss of the outer layer except for a few remnants (arrows). (D) Detail of the sporocyst wall from a control oocyst showing the outer (O) and inner (I) layers of the wall. (E) Detail of the sporocyst wall from a bleached oocyst showing the retention of both the outer (O) and inner (I) layers for the wall. (Scale bar, 100 nm.)

biology, from single molecules measurements to cell–cell measurements (31, 41–47). The sensitivity of force determination is usually limited by the thermal noise of the system and the properties of the chosen cantilever (30).

Here, we investigate, using AFM, the wall mechanics of T. gondii oocysts submitted to physical (heat inactivation) and chemical (bleach exposure) treatments separately or in combination to evaluate the contribution of each layer in the overall mechanics of the oocyst wall. Our results present a simple way to gently but firmly immobilize oocysts on surfaces to image them using fluorescence microscopy or test their mechanics using AFM under moderate forces. Our findings may be correlated to structural modifications of the oocyst wall and suggest a key biological role of the wall mechanics in maintaining the integrity of the T. gondii oocysts in the environment or exposed to disinfectants, therefore affecting potential infectivity to humans and animals.

Results

Microscopic Characteristics of T. gondii Oocysts Following Sporulation in Water. To evaluate the basic mechanics of the T. gondii oocyst wall, we limited the use of chemicals to avoid any modification of the wall structure because of handling or storage conditions. For this, oocysts were sporulated in water rather than in 2% (vol/vol) aqueous sulfuric acid solution, which is commonly used for oocyst sporulation and subsequent storage (11, 22, 48). After a 5-d sporulation process, the oocyst suspension contained 18.6 ± 2.7% of NS, 18.3 ± 6.4% of SB, and 63.0 ± 5.9% of SP oocysts (SI Appendix, Fig. S1). All these different oocyst subpopulations exhibited the same typical AF under UV excitation (SI Appendix, Fig. S1B). Careful observation, before and during AFM experiments, was a key step to the exact categorization of the objects.

Characterization of Bleach Effects on T. gondii Walls by EM. EM confirmed that control (H_2O-conserved) oocysts retained their typical double-layered wall (observed thickness ~ 50 nm, Fig. 1 A and B). In contrast, the outer layer (observed thickness ~ 18–20 nm) was absent in bleach-treated oocysts, with only the inner layer (observed thickness ~ 30 nm) remaining with, in certain cases, slight remnants of the outer layer persisting (Fig. 1C). The oocyst wall thicknesses that were observed here are con-sistent with but in the lower end of the values of such structures reported in literature (up to 100 nm for the bilayered wall) (24). The bilayered structure of the T. gondii sporocyst wall was maintained following bleach treatment of the oocyst wall (Fig. 1 D and E).

Characterization of T. gondii Walls by Fluorescence Microscopy. The properties of the wall of NS, SB, and SP oocysts were first assessed microscopically by analyzing their reactivity to the mAb 4B6, which is specific to the inner layer of the oocyst wall (49). To induce structural modifications of the bilayered oocyst wall, the parasites were treated with bleach to remove the outer layer and/or heated at 80 °C. In contrast to bleach treatment, heating oocysts at 80 °C efficiently kills the sporozoites; however, the effects on the wall structure remain largely unknown. Oocysts exposed only to water during their maturation and storage served as controls. The percentages of oocysts at different maturing stages exposing partially or totally their inner wall following these different surface treatments are shown in Fig. 2. Corresponding immunofluorescence and AF representative images are shown in SI Appendix, Fig. S2.

Between 21.2 and 25.6% of H_2O-exposed oocysts were labeled with antibody mAb 4B6 (Fig. 2). A mixture of unstained to totally mAb 4B6–stained oocysts was observed irrespective of the oocyst developmental stage (SI Appendix, Fig. S1A). Fluorescent staining appeared randomly distributed at the oocyst surface and ranged from almost continuous staining of the entire surface (SI Appendix, Fig. S2A, case 1) to very discrete patches (SI Appendix,

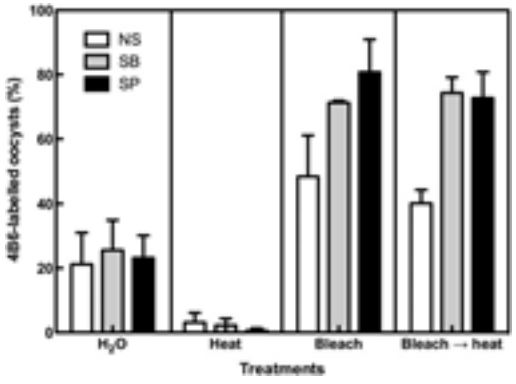

Fig. 2. Fluorescence labeling of the inner wall of T. gondii oocysts submitted to different surface treatments. NS, SB, and SP oocysts were bleached and/or heated before being allowed to react with 4B6 antibody specific to their inner wall (49, 58). The percentages of labeled parasites in each treatment condition are presented. No significant differences were observed between the stages of oocyst maturation for any given treatment. However, there were significant differences among treatments, with control H_2O oocysts differing from heated, bleached, and bleached then heated oocysts ($P < 0.001$–0.05) and heated oocysts differing from bleached, and bleached then heated oocysts ($P < 0.001$). No statistical difference was noted between bleached oocysts and bleached then heated oocysts at any maturing stage. The corresponding typical fluorescence images are presented in SI Appendix, Fig. S2.

Fig. S2A, case 2). In these conditions, 4B6 staining of the inner wall layer appeared to result from the infiltration of the antibody through cracks in the oocyst wall rather than the exposure of the outer aspect of the inner layer of the oocyst wall. This hypothesis was further supported by the fact that ~ 25–30% of H_2O-exposed oocysts were permeable to FITC in solution, again indicating possible openings in the oocyst wall (SI Appendix, Fig. S3). Irrespective of their 4B6 pattern, SB and SP oocysts were more autofluorescent than NS oocysts (SI Appendix, Figs. S2A and S4). Heating oocysts at 80 °C for 10 min led to a significant re-duction of the percentage of 4B6-positive oocysts at all matu-ration stages (0.6–3.1%) (Fig. 2). The few positive oocysts observed were very faintly stained in localized areas of the oocyst wall (SI Appendix, Fig. S2B). In these experimental conditions, heating did not appear to alter significantly the microscopic structure or internal content of NS, SB, and SP oocysts or the AF of the oocyst wall (SI Appendix, Fig. S2 B compared with A).

In contrast, there was a significant increase in mAb 4B6 staining of oocysts bleached with 3% bleach solution for 30 min (final mAb 4B6–labeled oocysts from 48.3 to 80.7% depending on the maturing stage) compared with control or heated oocysts (Fig. 2). In these experimental conditions, the antibody stained, at least partially, the inner layer of NS, SB, and SP oocyst wall usually with a strong intensity (SI Appendix, Fig. S2C), indicating that modifications of the wall structure increase the access of mAb 4B6 to the outer aspect of the inner layer of the wall, but not its infiltration through it because only ~ 25–30% of bleach-exposed oocysts were again permeable to FITC resulting from possible fractures in their wall (SI Appendix, Fig. S3). We also observed that several bleach-treated oocysts displayed a reduced AF pattern of the oocyst wall compared with the control oocysts (SI Appendix, Fig. S4), suggesting possible differences in the biochemical content of the oocyst wall between untreated and bleach-treated oocysts.

When bleached oocysts were subsequently heated at 80 °C, the percentages of mAb 4B6–positive parasites were similar to that observed with bleaching alone (40.1–74.3%) (Fig. 2). Microscopically, these oocysts had similar 4B6 and AF patterns compared with bleached-only oocysts, irrespective of the stage of maturation (SI Appendix, Fig. S2D compared with Fig. S2C). However, a few mAb 4B6–positive oocysts still had a very discrete wall AF (SI Appendix, Fig. S2D, case 5).

Attachment of the Oocysts for AFM Experiments. The mechanical properties of the wall of H_2O-stored, bleach-, and/or heat-treated oocysts at different maturing stages were then evaluated using AFM. For this, oocysts were first allowed to adhere onto poly-L-lysine (PLL)-coated glass microscopic slides before being approached by the AFM tip (SI Appendix, Fig. S5 A–C). We verified that the coating procedure on glass did not change significantly the initial observed proportions of the different subpopulations of the oocysts irrespective of their pretreatment SI Appendix, Fig. S5B). This coating procedure was suitable for firmly attaching the oocysts onto the glass surface, thus allowing repeated contacts between the AFM tip and each oocyst at a preset contact force of 1 nN. The fine positioning of the AFM tip on top of the substructures (i.e., sporocysts) does not largely affect the measurements (SI Appendix, Fig. S5 D and E).

Elastic Properties of the Oocyst Wall. Following our immobilization protocol, repeated force curves were obtained for each adhered object (Fig. 3 A and B). We observed that the indentation depth was <50 nm and typically ~ 20 nm (Fig. 3 C and D) irrespective of the maturing oocyst stages or its pretreatment (SI Appendix, Table S1). This median indentation is of the same order of magnitude as the most outer layer of the oocyst wall (20 nm) and smaller than the thickness of the most inner layer (30 nm) as measured in EM micrographs. Following this, (i) in absence of bleach treatment, we concluded that we measured the mechanics of, if not the outer layer alone, the bilayered structure of the wall, and (ii) following bleach treatment, we were able to access the mechanical properties solely of the inner layer of the wall.

Young moduli, E, obtained for NS, SB, and SP H_2O-stored oocysts were typically in the 10^6–10^7 Pa range and were not significantly different from each other (Fig. 3 E and F). Those elevated E values are similar to the ones reported for artificial polymeric capsules of comparable thicknesses (50). The median E moduli showed no significant variation between the different maturing oocyst stages irrespective of the oocyst pretreatment (SI Appendix, Tables S2 and S4). Force relaxation experiments during contact of the tip on the oocyst and the superposition of trace and retrace parts of the force curves indicated that no viscous behavior could be identified in this range of stimulations (Fig. 3 A and B). In addition, repetitions of contacts lead to rather unvarying indentation depths, with no apparent tendency of any plastic deformation of the oocyst wall for the investigated forces (Fig. 3C).

Pressing the oocysts at higher forces (30 or 120 nN) did not appear to strongly modify the mechanics of the oocyst wall (SI

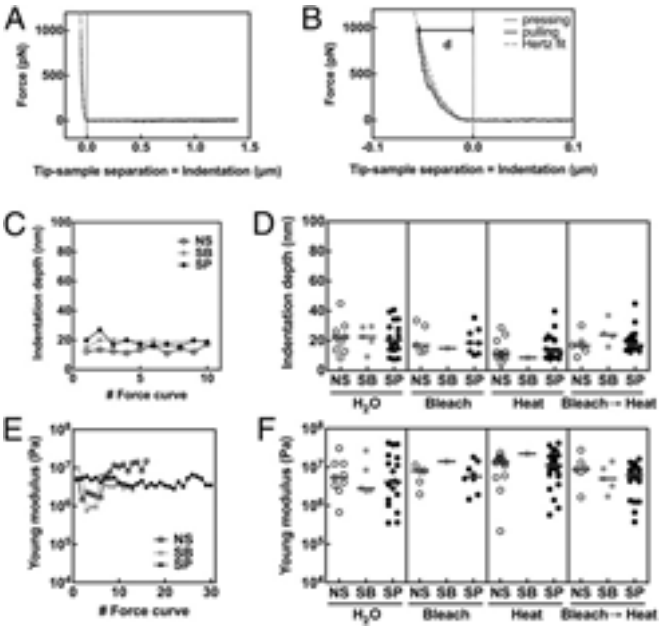

Fig. 3. Measuring mechanical properties of T. gondii oocysts. (A) Typical force curve (force vs. tip-sample separation) used for quantifying the Young modulus (note that pressing and pulling curves are almost superimposed). The dotted line is the point of contact. (B) Magnification of the contact region of the curves presented in A, showing the superimposition of pressing and pulling curves together with the Hertz fit described in the text (dotted line) and d as the maximal indentation. The superimposition of pressing and pulling curves shows that little if no dissipation is occurring in the material when indenting, ruling out any viscoelastic behavior under the conditions of our experiments. (C) Example of maximal indentation for untreated oocysts of different subtypes, showing no tendency upon repeated indentation. Note that 100 nm was used as the scale maximum because it is the upper bound of the thickness of the oocyst wall found in the literature. (D) Maximal indentation under a force of 1 nN as a function of oocyst subtype and treatment. (E) Repeated measured values of Young modulus of three untreated oocysts of various subtypes, showing that for a given object no tendency can be observed upon repeated indentation. Note that the value of 10^4 Pa used as the lower limit of the scale corresponds to the values recorded for hard eukaryotic cells as found in the literature. (F) Young modulus as a function of oocyst subtype and treatment. In D and F, each point is the median value obtained for a single oocyst upon successive indentations. The line is the median of the subsequent distribution. No significant differences are observed between the conditions for indentation (D and SI Appendix, Tables S1 and S4) or for Young modulus (F and SI Appendix, Tables S2 and S4).

Appendix, Fig. S5 F and G). However, in these conditions, we observed that oocysts were accidently removed from the slide because of the higher pressing force, making the AFM tip into a golf club and the oocyst the ball.

Adhesive Properties of the Oocyst Wall. In addition to indentation and elasticity measurements, the nonspecific adhesive properties of the oocyst wall were examined. Surface adhesion (Fig. 4) was measured as the force required to detach the AFM tip from the surface of the oocyst after indentation at 1 nN, with a fixed pulling speed of 1 μm/s. We observed that at least 50% of the force curves showed some adhesion (Fig. 4 A vs. B). The proportion of oocysts showing a detectable adhesion was observed to depend on the developmental stage and on the treatment of the oocyst surface. Temperature alone lowered the proportion of oocysts with adhesive surface properties, whereas application of bleach increased it (Fig. 4 C and D). Upon repeated pulling on the same object, adhesive forces did not show any marked tendency (Fig. 4E), indicating that materials coming from the wall did not pollute the tip. We observed that the strength of adhesion (i.e., the force required to fully detach the tip from the oocyst) was rather low (<100 pN) for control and temperature-treated oocysts but was significantly stronger when bleach was applied as a first treatment (Fig. 4F and SI Appendix, Table S3), suggesting important bleach-induced modifications of the wall. In conclusion, bleach treatment increases both the proportion of oocysts showing detectable adhesion and the overall strength of the adhesion, whereas high-temperature treatment alone did not affect adhesion force but reduced the proportion of oocysts showing significant adhesion.

Discussion

The T. gondii oocyst is a superstructure that protects the dormant but potentially infective sporozoites from many extreme conditions that would be deleterious for survival (24). Facing the external environment, the oocyst wall acts as a primary barrier to physical and chemical attacks as long as its complex polymeric organization is perfectly maintained (8, 12, 26). Different, but complementary, approaches have been applied to investigate the structure and molecular basis of the oocyst wall resilience, such as EM (9, 12, 24, 51) and proteomics studies (10, 12). However, oocysts are technically difficult to process for EM examination because of the impervious nature of the walls and proteomics usually require large numbers of highly purified oocysts, which are difficult to obtain because oocysts cannot be generated in vitro. Here, we addressed the structure and chemistry of each oocyst wall layer through measurement of their respective mechanical properties by combining wall treatments, fluorescence and EM observations, and AFM techniques on immobilized parasites.

In coccidian parasites such as T. gondii, the oocyst wall results from the particular arrangement of structural proteins through a sclerotization process involving both quinone tanning and protein dityrosine cross-linking and dehydration (12, 26). This process probably takes place very early in the development of the oocyst wall, from the NS stage before it leaves the host (21), and is thought to lead to hardened structures, which excludes water-soluble molecules to form a complex polymeric covering capable of resisting extended physical and chemical-induced disorganization. Interestingly, it has been recently claimed that the inner wall layer of Eimeria tenella oocysts possesses discrete pores of 5–250 nm (9). However, such structures in the T. gondii oocyst wall were not observed in the present or previous studies (26).

The oocyst wall layers in T. gondii are assumed to differ in their thickness and molecular content, the inner one being thicker, less electron-dense and more resistant to chemical degradation than the outer one (8). Using fluorescence imaging and EM combined with different treatments, we provide insights on the structure and chemistry of the wall of T. gondii oocysts. Specific immunostaining of the inner wall layer of H_2O-exposed oocysts was infrequent and appeared to result from the infiltration of the antibody through focal openings of the oocyst wall rather than exposure of the external surface of the inner layer. After heating, antibody staining was significantly decreased in control oocysts, whereas it had little, if no, effect on bleach-treated oocysts. This would suggest that heating is not denaturing the antigen recognized by the antibody and probably results from heat-induced reticulation of poly-protein structures of the outer layer reducing penetration of the antibody. In contrast, bleach treatment clearly affected both the structure and chemistry of the oocyst wall by removing the outer layer as seen in our EM micrographs and significantly affecting the oocyst wall AF. Consequently, most of the 4B6 staining observed in bleached oocysts could be linked to the exposure of the external surface of the inner layer of the oocyst wall.

Then, we investigated the mechanical properties of the double-layered oocyst wall and then those specific to the inner layer after removing the outer layer by treatment with bleach. We observed high E moduli comparable to polymeric shells (50), with neither viscous nor plastic behaviors. The E moduli were not significantly different between the different maturing stages and treatments involving temperature and bleach (alone or in combination). Considering the small indentation and high E modulus, our results strongly support that the global stiffness of the bilayered oocyst wall is in the same order as that of the inner layer alone. Interestingly, we showed that the oocyst wall stiffness did not vary significantly following parasite incubation at

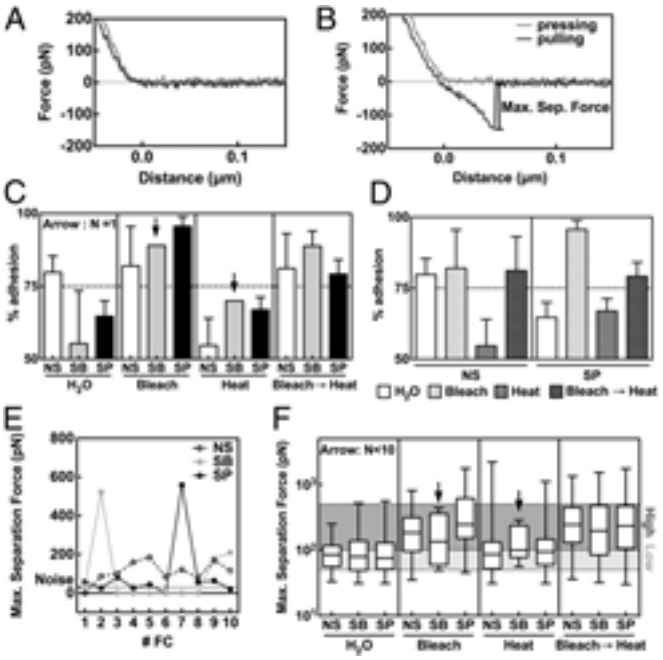

Fig. 4. Measuring nonspecific adhesive properties of T. gondii oocysts. (A) Typical force curve showing no adhesion event. (B) Typical force curve showing adhesion event. Magnification of the force curve near the contact/adhesion zone, with the recorded maximal adhesion force. The noise is far below the forces measured (typically 15–30 pN). (C) The fraction of adhesion as a function of oocyst subtypes and treatments (mean ± SD over the different days of experiments). Arrows show cases in which only one object for a given condition was observed over different repetitions. The dotted line has been placed at 75% adhesion as a guide for the eye. (D) Same data as in C, showing the comparison of NS and SP oocysts as a function of treatment. (E) Example of maximal separation force for untreated oocysts of different subtypes, showing no tendency upon repeated indentation/pulling, indicating that no strong pollution of or transfer of material to the lever tip was observed. The dotted line corresponds to the average observed noise on the baseline of the force curves. (F) Distribution of adhesion forces as whisker plots for oocysts of different subtypes and treatments. The significant differences correspond to the high- and low-adhesion separation on the graph (SI Appendix, Tables S3 and S4).

80 °C, which was quite unexpected because heat-induced stresses usually result in increasing stiffness of polymeric multilayer microcapsules from an increased shell thickness or reticulation (52). The conservative hypothesis suggests that each wall layer retains its basic mechanical properties by maintaining to large extend its molecular architecture, even at this temperature.

Besides mechanical measurements, AFM has also permitted examination of the nonspecific adhesive properties of each layer of the wall. It was observed that the proportion of oocyst showing adhesive properties was lower, as was the strength of the adhesion (i.e., overall force needed to fully detach the tip from the oocyst) in parasites retaining their typical double-layered wall structure, whereas there was a higher proportion of oocysts with adhesive properties and stronger adhesion was recorded in oocysts exposing solely the inner wall layer (SI Appendix, Fig. S6). This contrasting behavior might indicate the existence of important differences regarding the biochemical nature of the molecules and/or their arrangement from one wall layer to the other resulting from oocyst treatments modulating the structure of the wall. We speculate an increasing number of residual polypeptidic chains resulting from removal of (most of, if not all) the outer layer of the wall (SI Appendix, Fig. S6). Such differences have also been hypothesized by others (10), based on proteomics analyses of purified wall fractions of T. gondii oocysts exposed or not to bleach. It is not yet clear whether these different adhesive properties play a role in the oocyst fate. Recent studies have shown that the negative charges covering the surface of the oocyst wall prevent, in most cases, any aggregation of the parasites with other particles, thus allowing the parasites to disperse freely in fresh water (8). Further investigations, in particular on molecule-specific adhesion and the effects of digestive enzymes found in the host's gut, are required to extend our study and refine the biological significance of the adhesive properties of the oocyst wall.

From a methodological point of view, this study proposes a simple but efficient way to immobilize hardened biological microparticles such as T. gondii oocysts on glass slides for investigating the biophysical properties of their multilayer wall by using AFM and fluorescence microscopy techniques. It opens the possibility of extending such studies to immobilized T. gondii sporocysts and to other environmentally resistant parasitic pathogens such as Cryptosporidium and Giardia (53–56).

In conclusion, our study demonstrates that the overall rigidity of the bilayered T. gondii oocyst wall is as high as common plastic materials and that the inner layer is as robust as the bilayered wall itself. These findings strongly suggest that the mechanical characteristics of the T. gondii oocyst wall sustain the survival of the enclosed sporozoites facing physical and chemical attacks outside the host. In particular, our results suggest that chlorine-based products used as surface disinfectants or for treating drinking water are ineffective for efficiently killing T. gondii oocysts because these compounds are not able to permeabilize or disrupt the oocyst wall. However, it is clear that these properties have to be circumvented following oocyst ingestion by the host to safely deliver the sporozoites near the enterocytes. Because chemicals are ineffective in breaking the oocyst wall, a supplementary physical stimulus (still to be determined) seems to be required to prime oocyst-related infections in humans and animals.

Materials and Methods

Oocyst Purification and Sporulation. Oocysts of the genotype II TgNmBr1strain of T. gondii (57) were harvested from feces of cat 6–8 d after feeding infected mouse tissues to a T. gondii–free cat (1), then purified by flotation, and allowed to sporulate at room temperature (RT) for 5 d. Oocyst suspension was stored in distilled water at 4 °C until used within 3 mo. More details can be found in the SI Appendix.

Chemical and Physical Treatment of the Oocysts. Bleach treatment. H_2O-stored oocysts were washed three times in PBS at 5000 × g 5 min and then incubated with 1 mL of bleach solution containing 3% sodium hypochlorite (Fouque Chimie Service) in PBS for 30 min at 4 °C. The oocysts were then washed three times in PBS to remove bleach before being immobilized on coverslips for AFM experiments.

Heat inactivation. H_2O- or bleach-treated oocysts were washed three times in PBS at 5,000 × g for 5 min, resuspended in 500 μL PBS, and then placed in a dry block heater for 10 min at 80 °C to allow their inactivation before AFM experiments.

EM. Samples of water maintained and bleached oocysts were mechanically ruptured before fixation in 2.5% glutaraldehyde in 0.1 M phosphate buffer and processed for routine EM. In summary, the samples were postfixed in osmium tetroxide, dehydrated in ethanol, treated with propylene oxide, and embedded in Spurr's epoxy resin. Thin sections were cut and stained with uranyl acetate and lead citrate before examination in a Jeol 1200EX electron microscope.

Immunofluorescence assay. The effects of bleach and heat treatments on the integrity of the oocyst wall were evaluated by immunofluorescence assay combined with the AF. We labeled oocysts in suspension using a monoclonal antibody (IgM mAb 4B6), which was previously shown to react mainly with the inner layer of the oocyst wall (49, 58). More details can be found in the SI Appendix.

FITC infiltration assay. The permeability of the wall of oocysts exposed or not to bleach treatment was assessed by incubating oocysts with FITC at 0.5 mg/mL in PBS for 1 h at RT. Oocysts were subsequently washed four times in PBS by gentle centrifugations at 5,000 × g for 5 min and examined for fluorescence of FITC bound to internal proteins (SI Appendix, Fig. S3).

Measurements of the oocyst wall autofluorescence intensity. The effects of bleach treatment on the autofluorescence pattern of the oocyst wall were evaluated on AF gray scale images as described in SI Appendix, Fig. S4.

AFM Experiments. Oocyst immobilization on glass cover slides. Clean glass cover slides were coated with PLL after activation using residual air-based plasma. After rinsing and mounting on an observation chamber, a diluted suspension of untreated, heat-inactivated, or bleach-treated oocysts was seeded onto the PLL-treated zone and left to settle for 45 min to 1 h at RT before removal of nonadherent objects. We observed that this procedure did not grossly affect the different subpopulations ratios compared with the original suspension (SI Appendix, Fig. S5B). More details can be found in the SI Appendix.

AFM measurements. A Nanowizard I (JPK Instruments, used in closed loop mode) sitting on an Axiovert 200 (Zeiss) equipped with 10× and 40× lenses (with an optional 1.6× lens) was used to measure the oocyst mechanics. The system was sitting on an active damping table (Halcyonics) to suppress mechanical noise. Blunt AFM levers (MLCT, Veeco, nominal spring constant 10 pN/nm) were used and calibrated in situ. The spring constant (~ 15–18 pN/ nm) was determined in situ using a built-in thermal calibration method, far from the glass surface to avoid any hydrodynamical bias from the coupling with the substrate (59).

Using bright field, a given oocyst was chosen and a calibrated AFM cantilever was positioned on top of it (SI Appendix, Fig. S5 C and D). We checked that the measurements were not affected by the fine positioning of the tip on top of the structures (e.g., over the two substructures of SP oocysts and between them), so only the mid position was used to quantify the structure's mechanics (SI Appendix, Fig. S5 D and E).

At least 10 force curves, with a preset contact force of 1 nN, a preset contact time of 0 s, pressing/pulling speeds of 1 μm/s and an acquisition frequency of 1024 Hz, were acquired per oocyst (Fig. 3 A and B). Each force curve was evaluated by eye and processed on a PC using the built-in JPK IP software (JPK Instruments), resulting in three to more than 15 data points extracted for each structure. We first observed that the maximal indentation depth at 1 nN was on average ~ 20 nm (Fig. 3 C and D); this was less than the thickness of the bilayered wall structure, so the model was accurate enough to allow us to extract the Young modulus of the structures, E, one per valid force curve. To quantify the mechanics, we used as a first approximation a Hertz model for contact to fit the pressing part of the force curves as-suming a pyramidal tip of $\alpha = 21°$ half angle and incompressibility of the material ($\nu = 0.5$) (37) (Fig. 3 A and B). Because the indentation was <50 nm, we also tried the Hertz model for a spherical indenter of 25–50 nm radius and found little difference in the quality of the fit and subsequently calcu-lated E moduli.

For adhesion measurements, we retrieved from the return/pulling part of the force curves the maximum detachment force (Fig. 4B) and frequency of adhesion events (i.e., the ratio between the number of force curves having adhesion divided by the total number of force curves taken into account) (Fig. 4 C and D). We then calculated median adhesion forces and plotted the

entire force distribution as whisker plots. We did not observe any tendency of adhesion force versus upon repetitions of tests (Fig. 4E).

Experiments lasted maximum 2 h at RT before changing the sample and the cantilever, with occasional supplementations of water to counteract the evaporation.

Data Processing and Statistical Analysis. The distributions of the pooled data being non-Gaussian, median values with data points and/or whisker plots were then plotted as a function of the oocyst stage and treatment using Prism 5.0 and 6.0 (GraphPad). The data sets were compared using nonparametric tests such as Kruskal–Wallis.

ACKNOWLEDGMENTS. We thank M.L. Dardé for providing 4B6 hybridoma and PARIS Biotech for continuous support. This work was supported by Aix-Marseille University (Préciput 2011 Program) and the Agence Nationale de la Recherche Jeunes Chercheuses Jeunes Chercheurs DissecTion Program (P.-H.P.). P.H.P. thanks JPK Instruments for continuous support.

1. Dubey J (2010) Toxoplasmosis of Animals and Humans (CRC Press, Boca Raton, FL), 2nd Ed, pp 1–313.
2. Bahia-Oliveira LMG, et al. (2003) Highly endemic, waterborne toxoplasmosis in north Rio de Janeiro state, Brazil. Emerg Infect Dis 9(1):55–62.
3. de Moura L, et al. (2006) Waterborne toxoplasmosis, Brazil, from field to gene. Emerg Infect Dis 12(2):326–329.
4. Jones JL, Dubey JP (2010) Waterborne toxoplasmosis—recent developments. Exp Parasitol 124(1):10–25.
5. Boyer K, et al.; Toxoplasmosis Study Group (2011) Unrecognized ingestion of Toxoplasma gondii oocysts leads to congenital toxoplasmosis and causes epidemics in North America. Clin Infect Dis 53(11):1081–1089.
6. Dattoli VCC, et al. (2011) Oocyst ingestion as an important transmission route of Toxoplasma gondii in Brazilian urban children. J Parasitol 97(6):1080–1084.
7. Robert-Gangneux F, Dardé M-L (2012) Epidemiology of and diagnostic strategies for toxoplasmosis. Clin Microbiol Rev 25(2):264–296.
8. Dumètre A, et al. (2012) Interaction forces drive the environmental transmission of pathogenic protozoa. Appl Environ Microbiol 78(4):905–912.
9. Bushkin GG, et al. (2012) β-1,3-glucan, which can be targeted by drugs, forms a trabecular scaffold in the oocyst walls of Toxoplasma and Eimeria. mBio 3(5):e00258-12.
10. Fritz HM, Bowyer PW, Bogyo M, Conrad PA, Boothroyd JC (2012) Proteomic analysis of fractionated Toxoplasma oocysts reveals clues to their environmental resistance. PLoS ONE 7(1):e29955.
11. Fritz HM, et al. (2012) Transcriptomic analysis of toxoplasma development reveals many novel functions and structures specific to sporozoites and oocysts. PLoS ONE 7:2):e29998.
12. Mai K, et al. (2009) Oocyst wall formation and composition in coccidian parasites. Mem Inst Oswaldo Cruz 104(2):281–289.
13. Possenti A, et al. (2010) Molecular characterisation of a novel family of cysteine-rich proteins of Toxoplasma gondii and ultrastructural evidence of oocyst wall localisation. Int J Parasitol 40(14):1639–1649.
14. Dumètre A, et al. (2008) Effects of ozone and ultraviolet radiation treatments on the infectivity of Toxoplasma gondii oocysts. Vet Parasitol 153(3-4):209–213.
15. Wainwright KE, et al. (2007) Chemical inactivation of Toxoplasma gondii oocysts in water. J Parasitol 93(4):925–931.
16. Wainwright KE, et al. (2007) Physical inactivation of Toxoplasma gondii oocysts in water. Appl Environ Microbiol 73(17):5663–5666.
17. Villegas EN, et al. (2010) Using quantitative reverse transcriptase PCR and cell culture plaque assays to determine resistance of Toxoplasma gondii oocysts to chemical sanitizers. J Microbiol Methods 81(3):219–225.
18. Ware MW, et al. (2010) Determining UV inactivation of Toxoplasma gondii oocysts by using cell culture and a mouse bioassay. Appl Environ Microbiol 76(15):5140–5147.
19. Dubey JP, Frenkel JK (1972) Cyst-induced toxoplasmosis in cats. J Protozool 19(1): 155–177.
20. Ferguson DJ, Hutchison WM, Dunachie JF, Siim JC (1974) Ultrastructural study of early stages of asexual multiplication and microgametogony of Toxoplasma gondii in the small intestine of the cat. Acta Pathol Microbiol Scand B Microbiol Immunol 82(2): 167–181.
21. Ferguson DJ, Hutchison WM, Siim JC (1975) The ultrastructural development of the macrogamete and formation of the oocyst wall of Toxoplasma gondii. Acta Pathol Microbiol Scand [B] 83(5):491–505.
22. Dubey JP, Miller NL, Frenkel JK (1970) The Toxoplasma gondii oocyst from cat feces. J Exp Med 132(4):636–662.
23. Ferguson DJ, Birch-Andersen A, Siim JC, Hutchison WM (1979) Ultrastructural studies on the sporulation of oocysts of Toxoplasma gondii. III. Formation of the sporozoites within the sporocysts. Acta Pathol Microbiol Scand [B] 87(4):253–260.
24. Speer CA, Clark S, Dubey JP (1998) Ultrastructure of the oocysts, sporocysts, and sporozoites of Toxoplasma gondii. J Parasitol 84(3):505–512.
25. Dumètre A, Dardé ML (2003) How to detect Toxoplasma gondii oocysts in environmental samples? FEMS Microbiol Rev 27(5):651–661.
26. Belli SI, Smith NC, Ferguson DJP (2006) The coccidian oocyst: A tough nut to crack!. Trends Parasitol 22(9):416–423.
27. Dubey JP (1998) Toxoplasma gondii oocyst survival under defined temperatures. J Parasitol 84(4):862–865.
28. Belli SI, Wallach MG, Luxford C, Davies MJ, Smith NC (2003) Roles of tyrosine-rich precursor glycoproteins and dityrosine- and 3,4-dihydroxyphenylalanine-mediated protein cross-linking in development of the oocyst wall in the coccidian parasite Eimeria maxima. Eukaryot Cell 2(3):456–464.
29. Lindquist HDA, et al. (2003) Autofluorescence of Toxoplasma gondii and related coccidian oocysts. J Parasitol 89(4):865–867.
30. Franz C, Puech P-H (2008) Atomic force microscopy: A versatile tool for studying cell morphology, adhesion and mechanics. Cell Mol Bioeng 1(4):289–300.
31. Müller DJ, Dufrêne YF (2011) Force nanoscopy of living cells. Curr Biol 21(6): R212–R216.
32. Müller DJ, Krieg M, Alsteens D, Dufrêne YF (2009) New frontiers in atomic force microscopy: Analyzing interactions from single-molecules to cells. Curr Opin Biotechnol 20(1):4–13.
33. Müller DJ, Dufrêne YF (2008) Atomic force microscopy as a multifunctional molecular toolbox in nanobiotechnology. Nat Nanotechnol 3(5):261–269.
34. Friedrichs J, Taubenberger A, Franz CM, Muller DJ (2007) Cellular remodelling of individual collagen fibrils visualized by time-lapse AFM. J Mol Biol 372(3):594–607.
35. Muller DJ (2008) AFM: A nanotool in membrane biology. Biochemistry 47(31): 7986–7998.
36. Müller DJ, et al. (2006) Single-molecule studies of membrane proteins. Curr Opin Struct Biol 16(4):489–495.
37. Radmacher M (2002) Measuring the elastic properties of living cells by the atomic force microscope. Methods Cell Biol 68:67–90.
38. Radmacher M (2007) Studying the mechanics of cellular processes by atomic force microscopy. Methods Cell Biol 83:347–372.
39. Milosavljevic N, et al. (2010) Nongenomic effects of cisplatin: Acute inhibition of mechanosensitive transporters and channels without actin remodeling. Cancer Res 70:19):7514–7522.
40. Hampoelz B, et al. (2011) Microtubule-induced nuclear envelope fluctuations control chromatin dynamics in Drosophila embryos. Development 138(16):3377–3386.
41. Puech P-H, Poole K, Knebel D, Muller DJ (2006) A new technical approach to quantify cell-cell adhesion forces by AFM. Ultramicroscopy 106(8-9):637–644.
42. Fierro FA, et al. (2008) BCR/ABL expression of myeloid progenitors increases beta1-integrin mediated adhesion to stromal cells. J Mol Biol 377(4):1082–1093.
43. Taubenberger A, et al. (2007) Revealing early steps of alpha2beta1 integrin-mediated adhesion to collagen type I by using single-cell force spectroscopy. Mol Biol Cell 18(5): 1634–1644.
44. Franz CM, Taubenberger A, Puech P-H, Müller DJ (2007) Studying integrin-mediated cell adhesion at the single-molecule level using AFM force spectroscopy. Sci STKE 2007 (406):pl5.
45. Puech P-H, et al. (2011) Force measurements of TCR/pMHC recognition at T cell surface. PLoS ONE 6(7):e22344.
46. Puech P-H, et al. (2005) Measuring cell adhesion forces of primary gastrulating cells from zebrafish using atomic force microscopy. J Cell Sci 118(Pt 18):4199–4206.
47. Ulrich F, et al. (2005) Wnt11 functions in gastrulation by controlling cell cohesion through Rab5c and E-cadherin. Dev Cell 9(4):555–564.
48. Ferguson DJ, Birch-Andersen A, Siim JC, Hutchison WM (1979) Ultrastructural studies on the sporulation of oocysts of Toxoplasma gondii. I. Development of the zygote and formation of the sporoblasts. Acta Pathol Microbiol Scand [B] 87B(3):171–181.
49. Dumètre A, Dardé M-L (2007) Detection of Toxoplasma gondii in water by an immunomagnetic separation method targeting the sporocysts. Parasitol Res 101(4): 989–996.
50. Dubreuil F, Elsner N, Fery A (2003) Elastic properties of polyelectrolyte capsules studied by atomic-force microscopy and RICM. Eur Phys J E Soft Matter 12(2):215–221.
51. Dubremetz JF, Ferguson DJP (2009) The role played by electron microscopy in advancing our understanding of Toxoplasma gondii and other apicomplexans. Int J Parasitol 39(8):883–893.
52. Delcea M, et al. (2010) Mechanobiology: Correlation between mechanical stability of microcapsules studied by AFM and impact of cell-induced stresses. Small 6(24): 2858–2862.
53. Byrd TL, Walz JY (2005) Interaction force profiles between Cryptosporidium parvum oocysts and silica surfaces. Environ Sci Technol 39(24):9574–9582.
54. Byrd TL, Walz JY (2007) Investigation of the interaction force between Cryptosporidium parvum oocysts and solid surfaces. Langmuir 23(14):7475–7483.
55. Considine RF, Dixon DR, Drummond CJ (2002) Oocysts of Cryptosporidium parvum and model sand surfaces in aqueous solutions: An atomic force microscope (AFM) study. Water Res 36(14):3421–3428.
56. Considine R, Dixon D, Drummond C (2000) Laterally-resolved force microscopy of biological microspheres-oocysts of Cryptosporidium parvum. Langmuir 16:1323–1330.
57. Dubey JP, et al. (2011) Isolation of viable Toxoplasma gondii from feral guinea fowl (Numida meleagris) and domestic rabbits (Oryctolagus cuniculus) from Brazil. J Parasitol 97(5):842–845.
58. Dumètre A, Dardé M-L (2005) Immunomagnetic separation of Toxoplasma gondii oocysts using a monoclonal antibody directed against the oocyst wall. J Microbiol Methods 61(2):209–217.
59. Butt H-J, Jaschke M (1995) Calculation of thermal noise in atomic force microscopy. Nanotechnology 6:1–7.

Supplement Information (SI) Appendix

Materials and Methods

Oocyst Purification and Sporulation. Oocysts of the genotype II TgNmBr1strain of *T. gondii* (1) were harvested from feces of cat 6-8 days after feeding infected mouse tissues to a *T. gondii* free cat. Oocysts were collected by flotation at 4°C from cat feces on a 1.15 specific gravity sucrose solution without phenol. Concentrated oocyst pellets were then resuspended in 5 mL of distilled water and sent with cold packs within 48 hours by FedEx from Beltsville, Maryland, USA to Marseille, France, for sporulation and further experiments. Upon arrival, oocysts were washed three times in distilled water, pelleted by centrifugation at 5000 g for 5 min at room temperature (RT, 20-22°C), then resuspended in 7 mL of distilled water, and transferred in a 100 mL small plastic container. Oocysts were allowed to sporulate at RT for 5 days under adequate aeration and gentle continuous shaking. Sporulation progress was monitored daily by examining a fraction of the suspension by using bright field and UV microscopy as described elsewhere (2, 3). Oocyst suspension was stored in distilled water at 4°C until used within 3 months.

Immunofluorescence Assay (IFA). The effects of bleach and heat treatments on the integrity of the oocyst wall were evaluated by IFA combined with the autofluorescent signal (AF). We used a monoclonal antibody (IgM mAb 4B6), which was previously shown to react mainly with the inner layer of the oocyst wall (4, 5). This labeling was performed on oocysts in suspension rather than on air-dried parasites because drying on slides frequently induces the opening of the oocyst wall, which invariably gives to the mAb 4B6 an access to the inner layer (4, 5).

Briefly, untreated (H_2O-stored), heat-inactivated and bleach-treated oocysts were allowed to react with mAb 4B6 diluted at 1:100 in PBS for 30 min at 37°C. Oocysts were subsequently washed three times in PBS by gentle centrifugations at 5000 g for 5 min prior to incubation with a goat fluorescein-isothiocyanate (FITC) conjugate anti-mouse IgM+IgG (50-011, Argene, France) diluted to 1:100 in PBS. After that, parasites were washed again three times in PBS using the same protocol. Samples are then mounted and examined on a BX51 microscope (Olympus, France) equipped with suitable epifluorescence filters for FITC and UV autofluorescence (AF) and 40x lens. Bright field, FITC and AF images were acquired using the fluorescence imaging

system Cell^{A} (Olympus, France) and quantified using ImageJ 1.46m. The normally blue AF signal (Fig. S1B) was placed in the red channel and the FITC in the green channel for more convenient merging when performing fluorescence colocalization (Fig. S2).

Oocyst Immobilization on Glass Coverslides. Coverslides were cleaned using a 10% v/v Helmanex (Helma) solution in water in an ultrasonic bath for 30 min at 60°C, subsequently separately rinsed using alternating baths of ethanol and MQ water (three of each). Then, a supplementary cleaning in MQ water in an ultrasonic bath for 30 min at 60°C was performed before a last rinsing step with MQ water prior to drying under an air flow. Coverslides were stored away from humidity and dust for up to two weeks before use. For coating with poly-L-lysine (PLL), clean coverslides were activated for 1 min using a residual air-based plasma cleaner and a PDMS stamp with a circular 8 mm in diameter hole was stuck on them. 100 µL of 0.01% PLL in water was added and incubated for 45 min to 1 hr at RT. Three rinsing with PBS were performed before gluing a plastic ring with vacuum grease after removal of the PDMS stamp. The resulting chamber was then filled with 1 mL PBS and 100 µL of untreated, heat-inactivated, or bleach-treated oocyst suspension were seeded onto the PLL treated zone and let to settle for 45min to 1 hr at RT. Three gentle rinsing steps, with 1mL PBS, were performed before mounting on the AFM. We observed that this procedure did not grossly affect the different sub-populations ratios as compared to the original suspension (Fig. S5B). Observation lasted for 2 hr maximum at RT with occasional supplementations of water to counteract the evaporation.

SI Appendix Figures

Figure S1: *Toxoplasma gondii* oocyst subpopulations obtained after 5 days of sporulation in water. The suspension contained a mixture of different maturing stages of oocysts. Observed unsporulated oocysts (NS, small arrowhead) were spherical and contained a single granular mass (which corresponds to the zygote (6)), almost filling the oocyst. Maturing oocysts containing two sporoblasts (SB, large arrowhead) were ovoid and harbored two spherical sporoblasts, each filled with granular material. Fully sporulated (SP) oocysts containing sporocysts (large arrow, and C) were ovoid in shape and had two fully developed sporocysts containing four sporozoites each. Additionally, oocysts at the SB-SP transition (small arrow), i.e. containing one sporoblast and one sporocyst, were sometimes observed and were further recorded as SB oocysts (e.g. in AFM experiments). Oocysts were observed under bright field (A) or UV excitation for recording their autofluorescence pattern (B). Note the presence of fecal contaminants on the bright field image. Scale bars = 10 µm. (C) Fully sporulated *Toxoplasma gondii* oocysts, under bright field, harboring two sporocysts containing four banana-shaped sporozoite forms of the parasite. At least one sporozoite is very distinct in the picture (arrow). Scale bar = 5 µm.

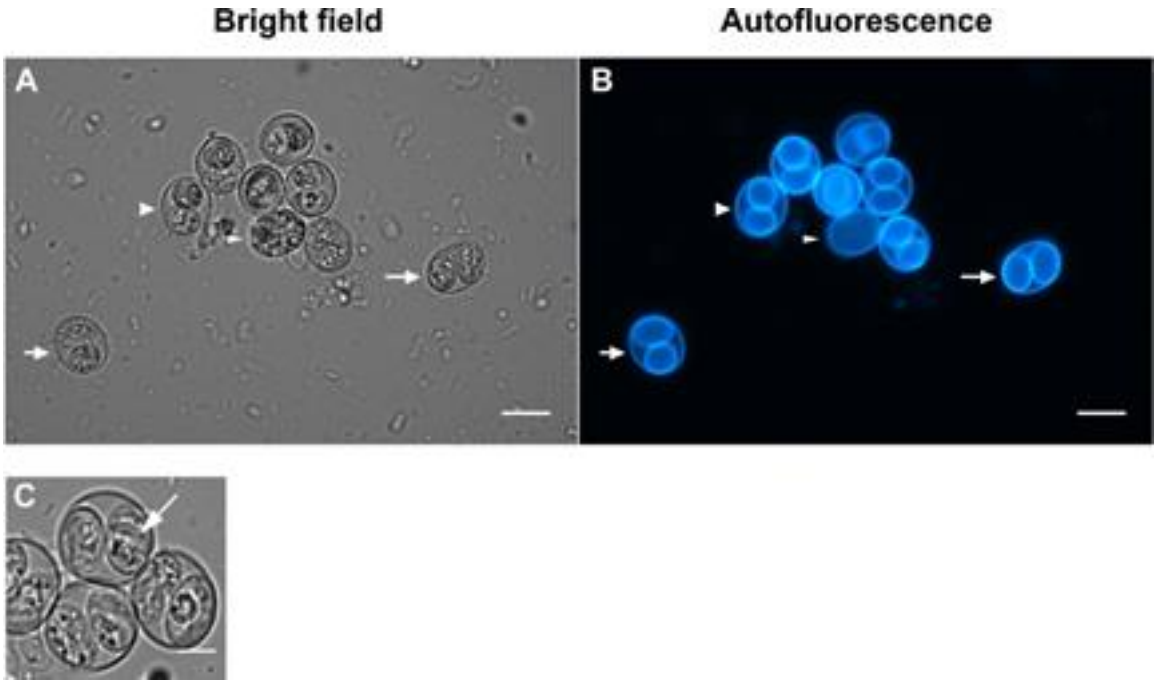

Figure S2: Fluorescence patterns of the wall of *T. gondii* oocysts exposed solely to H_2O (A), heated at 80°C (B), treated by bleach solution (C), or bleach- and then heat-treated (D) as described in the materiel and methods section. Oocysts were then allowed to react with 4B6 antibody specific to their inner wall (4, 5). BF, bright field; AF, autofluorescence under UV excitation (red channel); FITC corresponds to 4B6 fluorescence (green channel). Merge presents overlay between AF and FITC channel. Scale bars = 5 µm.

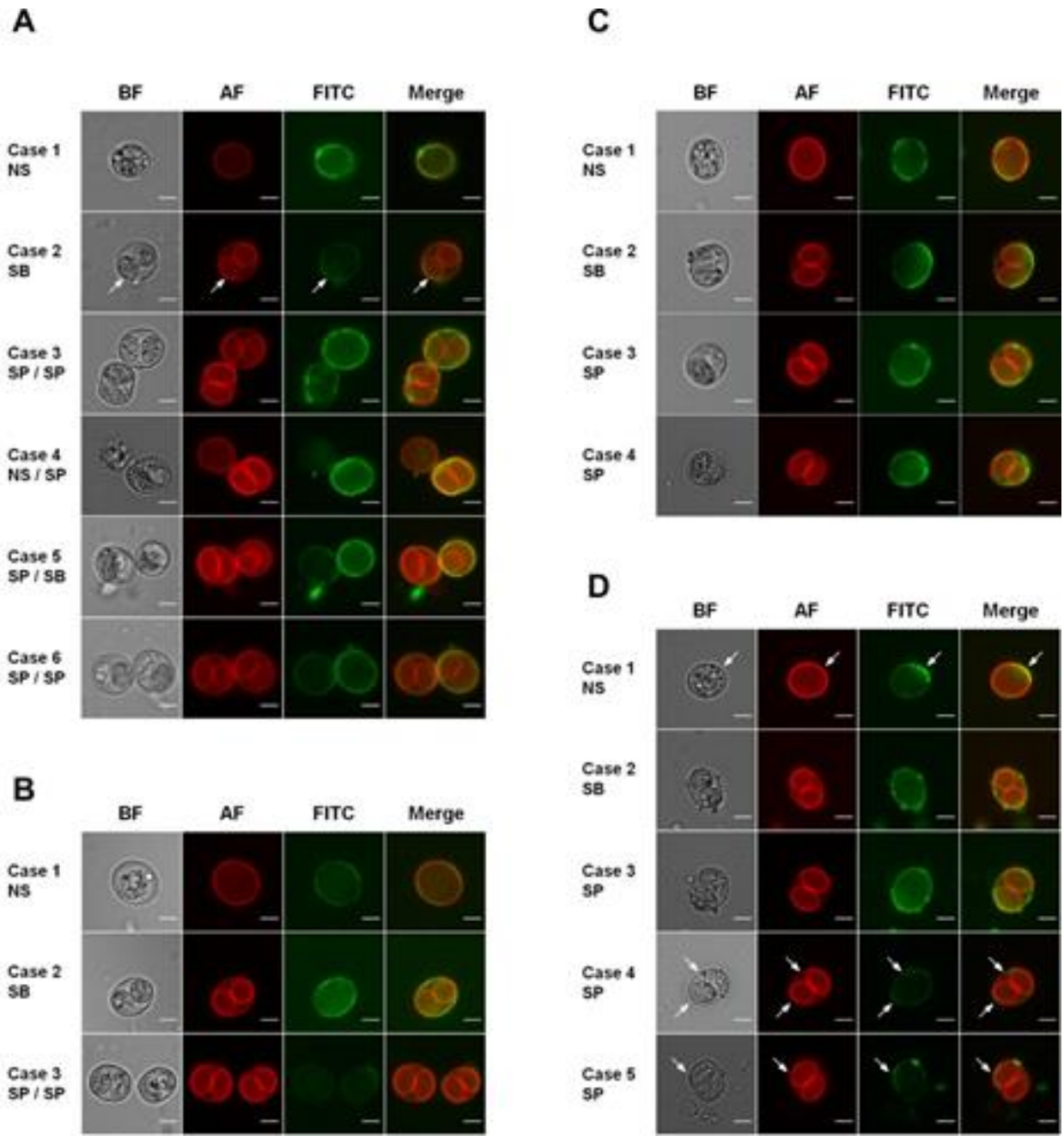
A
BF
AF
FITC
Merge
Case 1
NS
Case 2
SB
Case 3
SP / SP
Case 4
NS / SP
Case 5
SP / SB
Case 6
SP / SP
B
BF
AF
FITC
Merge
Case 1
NS
Case 2
SB
Case 3
SP / SP
C
BF
AF
FITC
Merge
Case 1
NS
Case 2
SB
Case 3
SP
Case 4
SP
D
BF
AF
FITC
Merge
Case 1
NS
Case 2
SB
Case 3
SP
Case 4
SP
Case 5
SP

Figure S3: Fluorescein Infiltration Assay. (A) The permeability of the wall of *Toxoplasma gondii* oocysts exposed or not to bleach treatment was assessed by incubating oocysts with fluorescein isothiocyanate. BF, bright field; AF, autofluorescence under UV excitation (red); FITC, fluorescein isothiocyanate fluorescence (green). Scale bars = 5 µm. (B) Percents of FITC permeable oocysts. No statistical difference was noted between control and bleach-treated oocysts at any maturing stage.

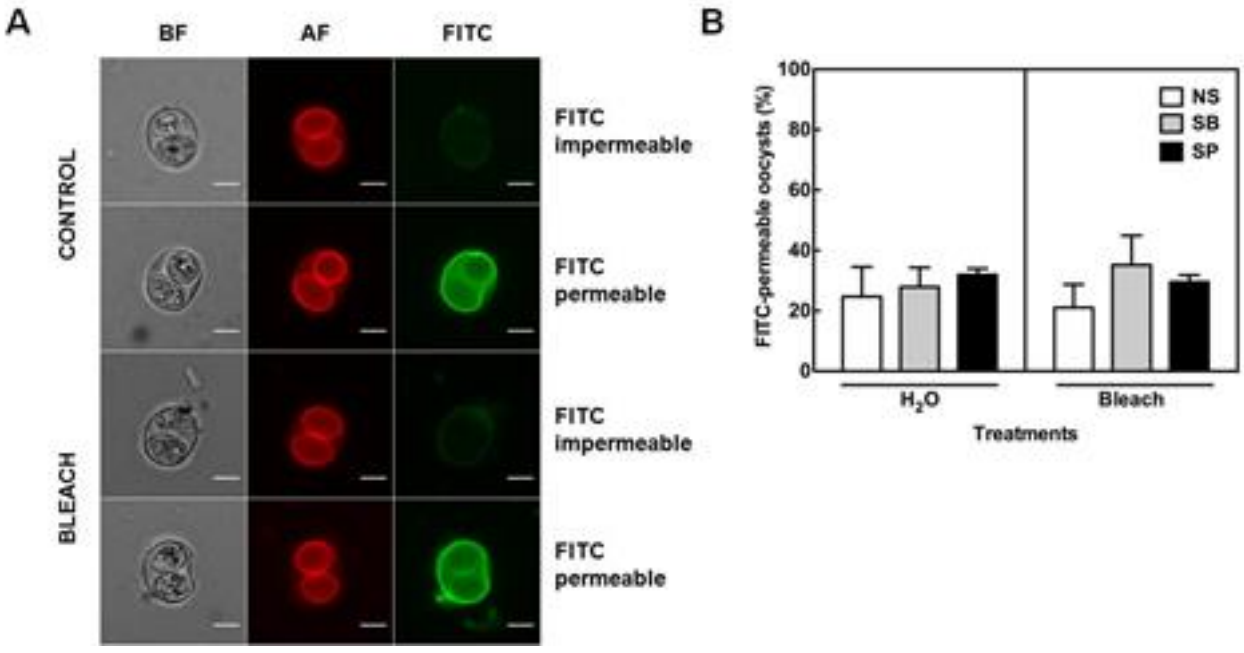

Figure S4: Quantification of the oocyst wall autofluorescence. (A) Control, heat- or bleach-treated oocysts were randomly examined microscopically under bright field (BF) and UV excitation (AF) (typically 10-35 oocysts per maturing stage and treatment condition). Their respective AF pattern was recorded as gray scale images. The relative oocyst wall AF intensity values were obtained by recording pixel gray values along a straight line (in yellow) arbitrarily set up across the width of each oocyst type. Values were plotted as a function of the pixel position along the selection line, and then normalized with regard to background gray value of each image (yellow square). Red circles indicate gray values of the oocyst wall that then were plotted in graph B. Scale bars= 5 µm. (B) Distribution of the relative autofluorescence intensity of the oocyst wall. The line is the median of the distribution. Significant differences were observed when comparing NS vs. NS/bleach ($p<0.001$), SB vs. SB/bleach ($p<0.001$), SP vs. SP/bleach ($p<0.001$), SB/heat vs. SB/bleach ($p<0.001$), and SP/heat vs. SP/bleach ($p<0.001$). No statistical difference was noted between control and heated oocysts at any maturing stage.

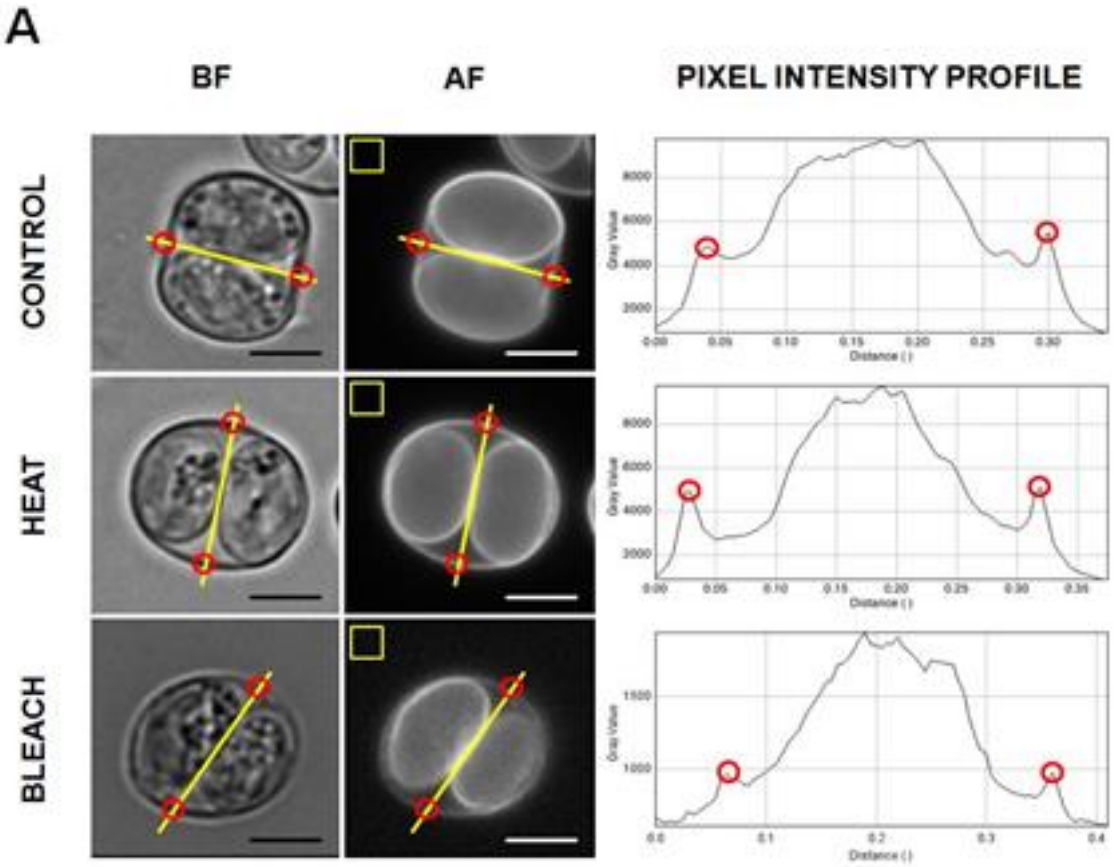
A
BF
AF
PIXEL INTENSITY PROFILE
CONTROL
HEAT
BLEACH
Gray Value
Distance ( )

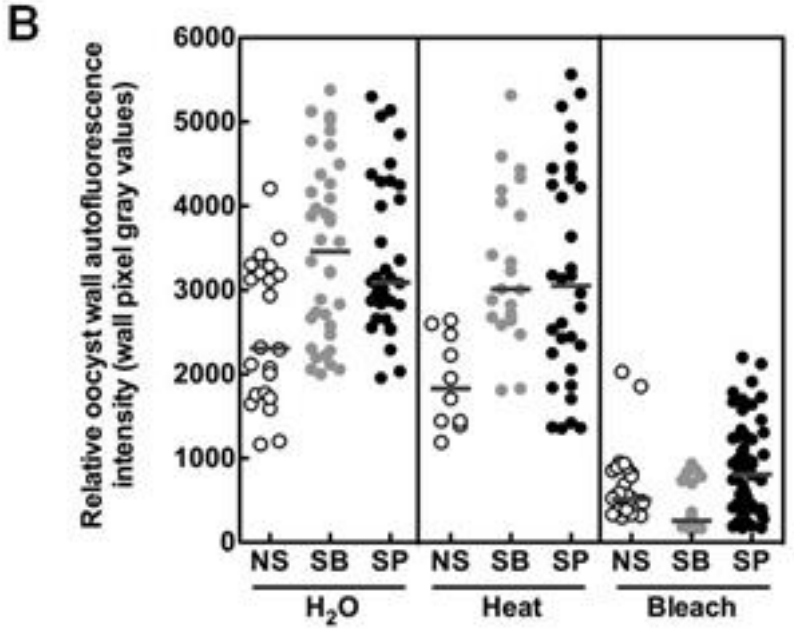
B
Relative oocyst wall autofluorescence intensity (wall pixel gray values)
6000
5000
4000
3000
2000
1000
0
NS SB SP NS SB SP NS SB SP
H2O
Heat
Bleach

Figure S5: Attachment of the *Toxoplasma gondii* oocysts onto Poly-L-Lysine (PLL)-coated glass slides and positioning of the AFM tip on top of the adhered oocysts. (A) Schematics of the procedure. (B) Conservation of subpopulations of oocysts after transfer to PLL-coated surface compared to the subpopulations of the parasites from the original suspension, as a fraction of total observed objects. (C) NS (left), SB (middle) and SP (right) oocysts were imaged together with the AFM cantilever (i.e. the dark triangular-shape object on the pictures), showing that one can distinguish them easily while doing AFM. The presence of other fecal objects such as yeasts or larger objects (mainly fiber-like debris, arrow) invariably occurred because the oocysts we used for AFM experiments were extracted and stored in water with no additional chemicals to limit bacterial proliferation. Such non-target objects could be located near the oocysts, at the same focal plane, however they did not affect the overall AFM cantilever motions, except on rare occasions. In these latter cases, the corresponding force curves were not processed for further analyses. Scale bars = 10 µm. (D) Zoom on the same SP oocyst as in panel C. The calibrated AFM cantilever was positioned using micrometer screws on top of it (e.g. over the two sporocysts of SP oocysts and between them (mid position)). (E) Distribution of the Young modulus at each of the three positions of the AFM tip. The red line is the median of the distribution. No significant difference was observed (Kruskall-Wallis test, $p>0.05$). No trace of the indentation can be seen in our optical magnification on the oocyst surface following indentation repetition. (F, G) Oocyst mechanics explored at higher contact forces. (F) Repeated measured values of Young modulus of 3 heated oocysts of two subtypes for heated oocyst samples, showing that for a given object no tendency can be observed when indenting with a maximal force 30 to 120 times the one used in our study. Note that the value of 10^4 Pa used as the lower limit of the scale corresponds to the values recorded for hard eukaryotic cells as found in literature. (G) Young modulus as a function of oocyst subtype. Each point is the value obtained for a single force curve. The red line is the median of the distribution. No significant difference is observed between the two cases and the measured medians are similar to the ones measured at 1 nN.

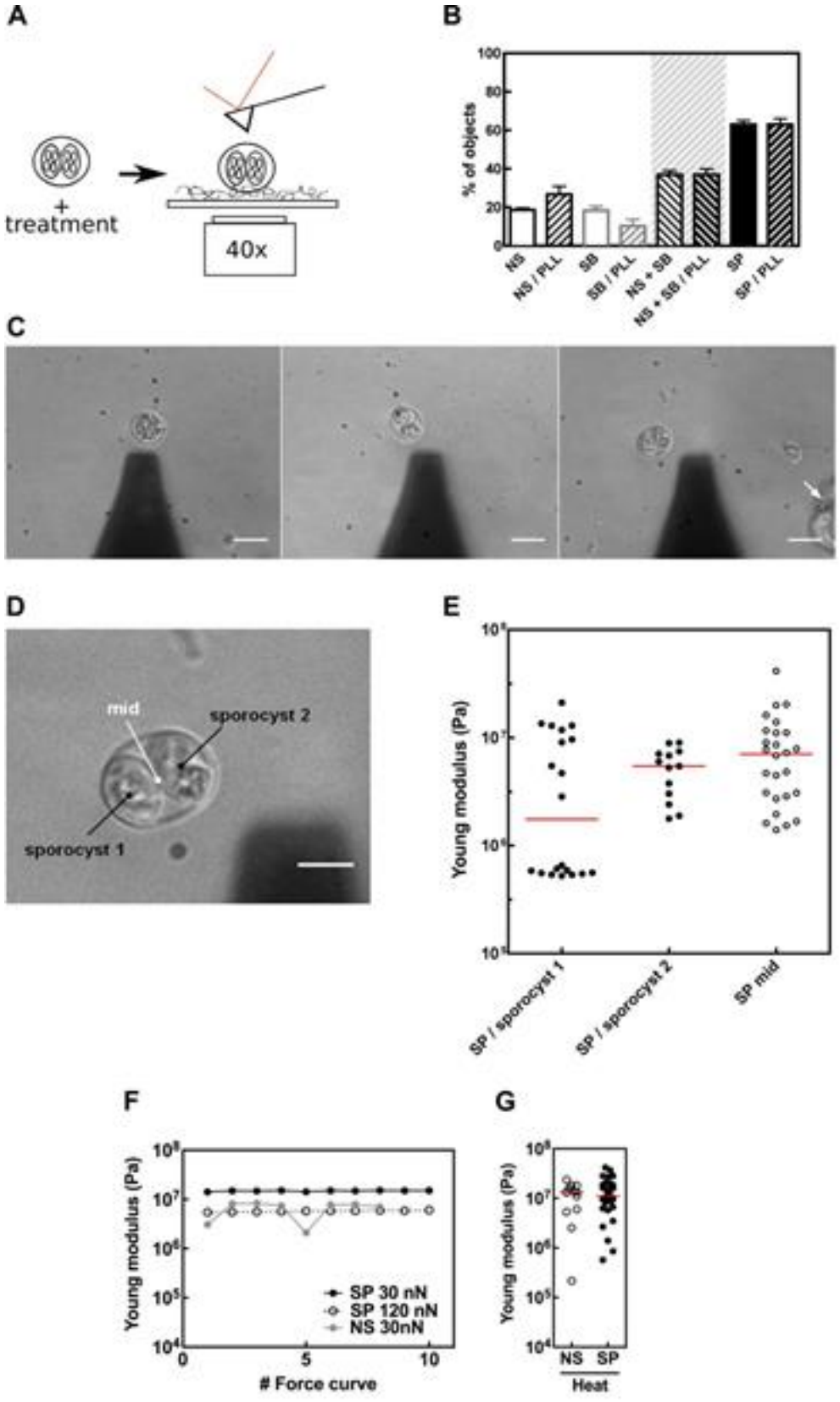
A
+
treatment
40x
B
% of objects
NS
NS / PLL
SB
SB / PLL
NS + SB
NS + SB / PLL
SP
SP / PLL
C
D
mid
sporocyst 2
sporocyst 1
E
Young modulus (Pa)
SP / sporocyst 1
SP / sporocyst 2
SP mid
F
Young modulus (Pa)
SP 30 nN
SP 120 nN
NS 30nN
Force curve
G
Young modulus (Pa)
NS
SP
Heat

Figure S6: Proposed structure of the bi-layered wall of the *Toxoplasma* oocyst in terms of mechanics and adhesive properties. Temperature and bleach treatments have no effect on the oocyst wall mechanics but have opposite effect on wall adhesion and accessibility to inner wall by a specific antibody: bleached oocysts exhibit higher adhesion frequency and forces than heated or control oocysts. Little differences are observed among the different maturing stages.

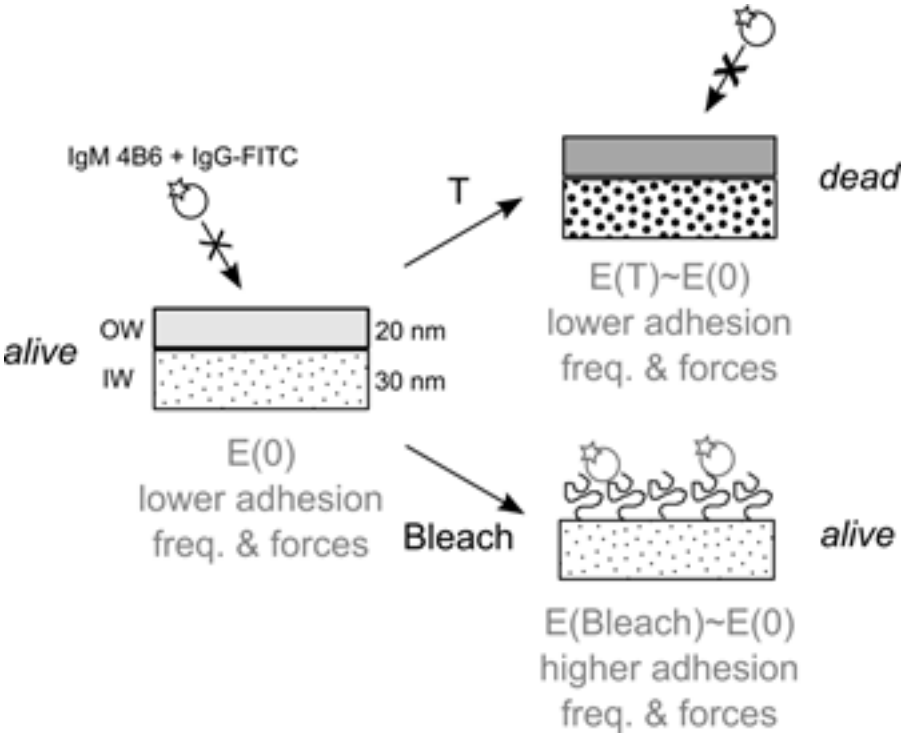

SI Appendix Tables

Table S1: Statistical analyses of the maximal indentation under a force of 1 nN as a function of oocyst subtype and treatment (see Fig. 3D). Data obtained with Prism 6 (GraphPad).

Table Analyzed	Indentation @ 1nN
Kruskal-Wallis test	
P value	0,0145
Exact or approximate P value?	Approximate
P value summary	*
Do the medians vary signif. (P < 0.05)	Yes
Number of groups	10
Kruskal-Wallis statistic	20,60

Data summary	
Number of treatments (columns)	10
Number of values (total)	115
Number of families	1
Number of comparisons per family	45
Alpha	0,05

Dunn's multiple comparisons test	Mean rank diff,	Significant?		Adjusted P Value
NS vs. SB	-2,622	No	ns	> 0,9999
NS vs. SP	1,861	No	ns	> 0,9999
NS vs. NS / T	33,46	No	ns	> 0,9999
NS vs. SP / T	30,20	No	ns	0,8379
NS vs. NS / bleach	1,778	No	ns	> 0,9999
NS vs. SP / bleach	7,340	No	ns	> 0,9999
NS vs. NS / bleach / T	13,94	No	ns	> 0,9999

NS vs. SB / bleach / T	-15,35	No	ns	> 0,9999
NS vs. SP / bleach / T	5,369	No	ns	> 0,9999
SB vs. SP	4,483	No	ns	> 0,9999
SB vs. NS / T	36,08	No	ns	> 0,9999
SB vs. SP / T	32,83	No	ns	> 0,9999
SB vs. NS / bleach	4,400	No	ns	> 0,9999
SB vs. SP / bleach	9,963	No	ns	> 0,9999
SB vs. NS / bleach / T	16,57	No	ns	> 0,9999
SB vs. SB / bleach / T	-12,73	No	ns	> 0,9999
SB vs. SP / bleach / T	7,991	No	ns	> 0,9999
SP vs. NS / T	31,60	No	ns	0,5983
SP vs. SP / T	28,34	No	ns	0,2352
SP vs. NS / bleach	-0,08333No	ns	> 0,9999	
SP vs. SP / bleach	5,479	No	ns	> 0,9999
SP vs. NS / bleach / T	12,08	No	ns	> 0,9999
SP vs. SB / bleach / T	-17,21	No	ns	> 0,9999
SP vs. SP / bleach / T	3,508	No	ns	> 0,9999
NS / T vs. SP / T	-3,256	No	ns	> 0,9999
NS / T vs. NS / bleach	-31,68	No	ns	> 0,9999
NS / T vs. SP / bleach	-26,12	No	ns	> 0,9999
NS / T vs. NS / bleach / T	-19,52	No	ns	> 0,9999
NS / T vs. SB / bleach / T	-48,81	No	ns	0,5487
NS / T vs. SP / bleach / T	-28,09	No	ns	> 0,9999
SP / T vs. NS / bleach	-28,43	No	ns	> 0,9999
SP / T vs. SP / bleach	-22,86	No	ns	> 0,9999
SP / T vs. NS / bleach / T	-16,26	No	ns	> 0,9999
SP / T vs. SB / bleach / T	-45,55	No	ns	0,4857
SP / T vs. SP / bleach / T	-24,84	No	ns	0,4285

NS / bleach vs. SP / bleach	5,563	No	ns	> 0,9999
NS / bleach vs. NS / bleach / T	12,17	No	ns	> 0,9999
NS / bleach vs. SB / bleach / T	-17,13	No	ns	> 0,9999
NS / bleach vs. SP / bleach / T	3,591	No	ns	> 0,9999
SP / bleach vs. NS / bleach / T	6,604	No	ns	> 0,9999
SP / bleach vs. SB / bleach / T	-22,69	No	ns	> 0,9999
SP / bleach vs. SP / bleach / T	-1,972	No	ns	> 0,9999
NS / bleach / T vs. SB / bleach / T	-29,29	No	ns	> 0,9999
NS / bleach / T vs. SP / bleach / T	-8,576	No	ns	> 0,9999
SB / bleach / T vs. SP / bleach / T	20,72	No	ns	> 0,9999

Table S2: Statistical analyses of the Young modulus as a function of oocyst subtype and treatment (see Fig. 3F). Data obtained with Prism 6 (GraphPad).

Table Analyzed	Young Modulus

Kruskal-Wallis test	
P value	0,0790
Exact or approximate P value?	Approximate
P value summary	ns
Do the medians vary signif. (P < 0.05)	No
Number of groups	10
Kruskal-Wallis statistic	15,46

Data summary	
Number of treatments (columns)	10
Number of values (total)	127
Number of families	1
Number of comparisons per family	45
Alpha	0,05

Dunn's multiple comparisons test	Mean rank diff,	Significant?		Adjusted P Value
SP / T vs. NS / T	2,998	No	ns	> 0,9999
SP / T vs. SP / bleach	25,15	No	ns	> 0,9999
SP / T vs. NS / bleach	28,15	No	ns	> 0,9999
SP / T vs. SP	25,97	No	ns	0,6446
SP / T vs. SB	30,15	No	ns	> 0,9999
SP / T vs. NS	26,65	No	ns	> 0,9999
SP / T vs. SP / bleach / T	29,03	No	ns	0,1485

SP / T vs. SB / bleach / T	29,75	No	ns	> 0,9999
SP / T vs. NS / bleach / T	11,32	No	ns	> 0,9999
NS / T vs. SP / bleach	22,15	No	ns	> 0,9999
NS / T vs. NS / bleach	25,15	No	ns	> 0,9999
NS / T vs. SP	22,97	No	ns	> 0,9999
NS / T vs. SB	27,15	No	ns	> 0,9999
NS / T vs. NS	23,65	No	ns	> 0,9999
NS / T vs. SP / bleach / T	26,03	No	ns	> 0,9999
NS / T vs. SB / bleach / T	26,75	No	ns	> 0,9999
NS / T vs. NS / bleach / T	8,321	No	ns	> 0,9999
SP / bleach vs. NS / bleach	3,000	No	ns	> 0,9999
SP / bleach vs. SP	0,8158	No	ns	> 0,9999
SP / bleach vs. SB	5,000	No	ns	> 0,9999
SP / bleach vs. NS	1,500	No	ns	> 0,9999
SP / bleach vs. SP / bleach / T	3,875	No	ns	> 0,9999
SP / bleach vs. SB / bleach / T	4,600	No	ns	> 0,9999
SP / bleach vs. NS / bleach / T	-13,83	No	ns	> 0,9999
NS / bleach vs. SP	-2,184	No	ns	> 0,9999
NS / bleach vs. SB	2,000	No	ns	> 0,9999
NS / bleach vs. NS	-1,500	No	ns	> 0,9999
NS / bleach vs. SP / bleach / T	0,8750	No	ns	> 0,9999
NS / bleach vs. SB / bleach / T	1,600	No	ns	> 0,9999
NS / bleach vs. NS / bleach / T	-16,83	No	ns	> 0,9999
SP vs. SB	4,184	No	ns	> 0,9999
SP vs. NS	0,6842	No	ns	> 0,9999
SP vs. SP / bleach / T	3,059	No	ns	> 0,9999
SP vs. SB / bleach / T	3,784	No	ns	> 0,9999
SP vs. NS / bleach / T	-14,65	No	ns	> 0,9999

SB vs. NS	-3,500	No	ns	> 0,9999
SB vs. SP / bleach / T	-1,125	No	ns	> 0,9999
SB vs. SB / bleach / T	-0,4000	No	ns	> 0,9999
SB vs. NS / bleach / T	-18,83	No	ns	> 0,9999
NS vs. SP / bleach / T	2,375	No	ns	> 0,9999
NS vs. SB / bleach / T	3,100	No	ns	> 0,9999
NS vs. NS / bleach / T	-15,33	No	ns	> 0,9999
SP / bleach / T vs. SB / bleach / T	0,7250	No	ns	> 0,9999
SP / bleach / T vs. NS / bleach / T	-17,71	No	ns	> 0,9999
SB / bleach / T vs. NS / bleach / T	-18,43	No	ns	> 0,9999

Table S3: Statistical analyses of the distribution of adhesion forces as whisker plots for oocysts of different subtypes and treatments (see Fig. 4F). Data obtained with Prism 6 (GraphPad).

Table Analyzed	Adhesion Force
Kruskal-Wallis test	
P value	< 0,0001
Exact or approximate P value?	Approximate
P value summary	****
Do the medians vary signif. (P < 0.05)	Yes
Number of groups	12
Kruskal-Wallis statistic	216,2

Data summary	
Number of treatments (columns)	12
Number of values (total)	913
Number of families	1
Number of comparisons per family	66
Alpha	0,05

Dunn's multiple comparisons test	Mean rank diff,	Significant?		Adjusted P Value
NS vs. SB	-15,39	No	ns	> 0,9999
NS vs. SP	-4,319	No	ns	> 0,9999
NS vs. NS / T	-42,15	No	ns	> 0,9999
NS vs. SB / T	-142,8	No	ns	> 0,9999
NS vs. SP / T	-60,13	No	ns	> 0,9999
NS vs. NS / bleach	-212,6	Yes	**	0,0017
NS vs. SB / bleach	-138,8	No	ns	> 0,9999
NS vs. SP / bleach	-332,5	Yes	****	< 0,0001

NS vs. NS / bleach / T	-308,4	Yes	****	< 0,0001
NS vs. SB / bleach / T	-237,1	Yes	****	< 0,0001
NS vs. SP / bleach / T	-278,8	Yes	****	< 0,0001
SB vs. SP	11,07	No	ns	> 0,9999
SB vs. NS / T	-26,76	No	ns	> 0,9999
SB vs. SB / T	-127,4	No	ns	> 0,9999
SB vs. SP / T	-44,74	No	ns	> 0,9999
SB vs. NS / bleach	-197,2	No	ns	0,0629
SB vs. SB / bleach	-123,4	No	ns	> 0,9999
SB vs. SP / bleach	-317,1	Yes	****	< 0,0001
SB vs. NS / bleach / T	-293,1	Yes	****	< 0,0001
SB vs. SB / bleach / T	-221,8	Yes	**	0,0087
SB vs. SP / bleach / T	-263,4	Yes	****	< 0,0001
SP vs. NS / T	-37,83	No	ns	> 0,9999
SP vs. SB / T	-138,4	No	ns	> 0,9999
SP vs. SP / T	-55,81	No	ns	> 0,9999
SP vs. NS / bleach	-208,2	Yes	***	0,0003
SP vs. SB / bleach	-134,5	No	ns	> 0,9999
SP vs. SP / bleach	-328,2	Yes	****	< 0,0001
SP vs. NS / bleach / T	-304,1	Yes	****	< 0,0001
SP vs. SB / bleach / T	-232,8	Yes	****	< 0,0001
SP vs. SP / bleach / T	-274,4	Yes	****	< 0,0001
NS / T vs. SB / T	-100,6	No	ns	> 0,9999
NS / T vs. SP / T	-17,98	No	ns	> 0,9999
NS / T vs. NS / bleach	-170,4	No	ns	0,0985
NS / T vs. SB / bleach	-96,67	No	ns	> 0,9999
NS / T vs. SP / bleach	-290,4	Yes	****	< 0,0001
NS / T vs. NS / bleach / T	-266,3	Yes	****	< 0,0001

NS / T vs. SB / bleach / T	-195,0	Yes	*	0,0109
NS / T vs. SP / bleach / T	-236,6	Yes	****	< 0,0001
SB / T vs. SP / T	82,64	No	ns	> 0,9999
SB / T vs. NS / bleach	-69,79	No	ns	> 0,9999
SB / T vs. SB / bleach	3,946	No	ns	> 0,9999
SB / T vs. SP / bleach	-189,7	No	ns	> 0,9999
SB / T vs. NS / bleach / T	-165,7	No	ns	> 0,9999
SB / T vs. SB / bleach / T	-94,38	No	ns	> 0,9999
SB / T vs. SP / bleach / T	-136,0	No	ns	> 0,9999
SP / T vs. NS / bleach	-152,4	Yes	*	0,0298
SP / T vs. SB / bleach	-78,69	No	ns	> 0,9999
SP / T vs. SP / bleach	-272,4	Yes	****	< 0,0001
SP / T vs. NS / bleach / T	-248,3	Yes	****	< 0,0001
SP / T vs. SB / bleach / T	-177,0	Yes	**	0,0011
SP / T vs. SP / bleach / T	-218,6	Yes	****	< 0,0001
NS / bleach vs. SB / bleach	73,73	No	ns	> 0,9999
NS / bleach vs. SP / bleach	-120,0	No	ns	0,7992
NS / bleach vs. NS / bleach / T	-95,88	No	ns	> 0,9999
NS / bleach vs. SB / bleach / T	-24,59	No	ns	> 0,9999
NS / bleach vs. SP / bleach / T	-66,22	No	ns	> 0,9999
SB / bleach vs. SP / bleach	-193,7	No	ns	> 0,9999
SB / bleach vs. NS / bleach / T	-169,6	No	ns	> 0,9999
SB / bleach vs. SB / bleach / T	-98,33	No	ns	> 0,9999
SB / bleach vs. SP / bleach / T	-139,9	No	ns	> 0,9999
SP / bleach vs. NS / bleach / T	24,08	No	ns	> 0,9999
SP / bleach vs. SB / bleach / T	95,36	No	ns	> 0,9999
SP / bleach vs. SP / bleach / T	53,74	No	ns	> 0,9999
NS / bleach / T vs. SB / bleach / T	71,29	No	ns	> 0,9999

NS / bleach / T vs. SP / bleach / T	29,67	No	ns	> 0,9999
SB / bleach / T vs. SP / bleach / T	-41,62	No	ns	> 0,9999

Table S4: Summary of median values of indentation, *E* moduli, and adhesion force of *Toxoplasma* oocysts at different maturing stages following different surface treatments. n = conserved data points.

	H_2O			Heat			Bleach			Bleach→heat		
	NS	**SB**	**SP**	**NS**	**SB**	**SP**	**NS**	**SB**	**SP**	**NS**	**SB**	**SP**
Indentation (nm)	22,5	22,6	20,5	11,4	8,60	12,4	17,0	15,0	18,5	16,8	23,9	17,1
n (oocysts)	9	5	18	11	1	27	5	1	8	6	4	22
***E* modulus (MPa)**	5.3	2.8	4.2	11.1	22.2	11.1	7.9	14.0	5.7	8.8	5.0	6.0
n (oocysts)	9	5	19	13	1	33	5	1	8	6	5	24
Adhesion force (pN)	85,0	79,5	75,5	86,0	100,0	94,5	184,5	134,5	246,0	244,5	197,0	234,0
n (force curves)	67	34	124	51	7	186	46	8	90	60	53	187

SI Appendix Reference list

1. Dubey JP et al. (2011) Isolation of viable *Toxoplasma gondii* from feral guinea fowl (*Numida meleagris*) and domestic rabbits (*Oryctolagus cuniculus*) from Brazil. *J Parasitol* 97:842–845.
2. Fritz HM et al. (2012) Transcriptomic analysis of *Toxoplasma* development reveals many novel functions and structures specific to sporozoites and oocysts. *PLoS ONE* 7:e29998.
3. Dubey JP, Miller NL, Frenkel JK (1970) The *Toxoplasma gondii* oocyst from cat feces. *J Exp Med* 132:636–662.
4. Dumètre A, Dardé M-L (2007) Detection of *Toxoplasma gondii* in water by an immunomagnetic separation method targeting the sporocysts. *Parasitol Res* 101:989–996.
5. Dumètre A, Dardé M-L (2005) Immunomagnetic separation of *Toxoplasma gondii* oocysts using a monoclonal antibody directed against the oocyst wall. *J Microbiol Methods* 61:209–217.
6. Ferguson DJ, Birch-Andersen A, Siim JC, Hutchison WM (1979) Ultrastructural studies on the sporulation of oocysts of *Toxoplasma gondii*. I. Development of the zygote and formation of the sporoblasts. *Acta Pathol Microbiol Scand B* 87B:171–181.